Received: 11 November 2022 | Revised: 31 January 2023 | Accepted: 18 February 2023

DOI: 10.1002/pc.27293

RESEARCH ARTICLE

Polymer COMPOSITES WILEY

Monitoring and verification of micro-strain generated inside the laminate subjected to thermal loading through fiber bragg grating sensors and classical laminate theory

Çağatay Yılmaz[1] | Hafiz Qasim Ali[2,3,4] | Mehmet Yıldız[2,3,4]

[1]Mechanical Engineering, Faculty of Engineering, Abdullah Gul University, Kayseri, Turkey

[2]Faculty of Engineering and Natural Sciences, Sabanci University, İstanbul, Turkey

[3]Integrated Manufacturing Technology, Research and Application Center, Sabanci University, Istanbul, Turkey

[4]Composite Technologies Center of Excellence, Sabanci University-Kordsa, Istanbul, Turkey

Correspondence
Çağatay Yılmaz, Mechanical Engineering, Abdullah Gul Universitesi, Kayseri, Turkey.
Email: yilmaz.cagatay@agu.edu.tr

Abstract

Fiber Bragg Grating (FBG) sensors possess enormous potential for the cure monitoring and integrity assessment of Carbon Fiber Reinforced Polymer (CFRP) composites. These sensors can be embedded inside the structure to monitor the strain in the desired region of interest. The strain on an FBG sensor can be calculated by measuring the change in the center wavelength of the sensor. This change in center wavelength is a function of temperature and mechanical strain. Therefore, temperature compensation is necessary for a precise mechanical strain measurement with an FBG sensor. In this study, FBG sensors are embedded in different layers of the CFRP laminate to record the mechanical strain caused by the thermal expansion, which happens under the influence of temperature. Classical laminate theory (CLT) is implemented to assess the accuracy of FBG sensor measurements and the strain data acquired from both FBG sensor and CLT correlates. Furthermore, a resistive strain gauge is deployed to measure the strain under the influence of temperature. It is depicted that strain values recorded by the strain gauge under the influence of the temperature do not agree with the strain measured by CLT, and an error of 150% occurs among their values.

KEYWORDS

carbon fiber laminated composite, classical lamination theory, fiber brag grating sensor, small strain measurement

1 | INTRODUCTION

Carbon fiber-reinforced polymeric (CFRP) laminated structures have attracted the attention of the aerospace industry in the past decade due to their high specific strength and modulus values compared to their traditional metallic counterpart, such as aluminum.[1–3] Although these CFRPs are widely used in the aerospace industry. But still, strain measurement and validation among different layers of these laminates is a matter of concern because of processing and environmental factors, such as temperature, which cause a significant difference. To overcome this issue, one of the most promising sensor-based approach to measure strain in the different layers of CFRP is the Fiber Bragg Grating (FBG) sensor.

FBG sensors have an immense potential to monitor the curing process and residual stress measurement due to the shrinkage of epoxy resin.[4–8] Dunphy et al.[9] and Murukeshan et al.[10] utilized the FBG sensors for cure monitoring, where the change in the center wavelength of the FBG sensor is tracked to both monitors the vitrification and curing of thermoset composite. K Jung et al.[11]

embedded an FBG sensor into the 3-D hybrid braided composite tube. Curing behavior and the mechanical strain of the tube under the compression and flexural loads are investigated once it is cured. Along with the temperature changes, the contraction and expansion caused by the curing of the matrix are measured efficiently. In another study, the cure and flow monitoring of resin transfer molded GFRP using the FBG sensor is monitored, and it is shown that the results obtained by the FBG sensors are also validated by etched bare fiber optic sensor and Fresnel-based refractometer.[12] In compelling research conducted by Colpo et al.,[13] an FBG sensor is inscribed on a technical textile glass fiber. The glass fiber was simultaneously used as a reinforcing agent and a sensor to monitor the residual stresses in a single fiber composite. Yadav et al.[14] studied the effectiveness of fiber Bragg grating sensors for monitoring residual strains for carbon fiber-reinforced thermoplastic automated tape layup. A cure monitoring system is designed using the FBG sensor to find the best curing cycle, which results in the least amount of residual thermal stress in CFRP materials.[15] Similarly, an FBG sensor is used to investigate the curing process of a cross-ply CFRP material in an autoclave to decrease residual thermal stress.[16]

Apart from monitoring the manufacturing of composite materials, these FBG sensors have been extensively used for the structural health monitoring of laminated composite materials. Keulen et al.[17] deployed FBG sensors for strain measurement during the fatigue testing of composite materials to predict the remaining useful life of glass fiber-reinforced polymeric (GFRP) materials. The damage accumulation of the GFRP under the static and quasi-static tensile test is monitored through a biaxial FBG sensor.[18] Akay et al.[19] measured the reduction in Poisson's ratio of GFRP composites under fatigue loading using the strain readings of biaxially embedded FBG sensors. The Poisson's ratio depreciates as the damage accumulates during the cyclic loading. Similarly, in another study, FBG sensors monitor the health of a composite structure bonded on the metallic substrate.[20] Mohanta et al.[21] used an embedded FBG sensor to monitor the long-term degradation of epoxy–glass composite in corrosive water. It is found that the long-term stability can be effectively monitored by tracking the hygrothermal strain developed on the specimens immersed in corrosive produced waters.

Crack detection is another promising application area where FBG sensors are the potential candidate for deployment. Imminent fracture in biaxial GFRP material under a tension-tension fatigue loading is predicted by using a multiplexed FBG sensor on a single fiber optic cable.[22] Kocaman et al.[23] monitored the failure modes of foam core sandwich composites by using the spectrum and center wavelength of the FBG sensor. It is shown that depending on the damage type, the response of the FBG sensor varies. In addition to detecting crack formation with the FBG sensor, another attractive sensing capacity of the FBG is the quantification of self-healing[24] as well as impact localization for self-healing.[25] The possible application of the FBG sensors can be even broadened to shape sensing for composite structures.[26,27]

Measuring the strain on the individual layers within a composite laminate with an FBG sensor is the main versatility and advantage of the FBG sensor. The FBG sensors are capable of measuring the strain state of the individual layers within the composite laminate under a particular loading condition. Most of the research in the literature with FBG sensors focuses on the measurement of global strain for composite laminates.[17,28] However, when the dimension and embeddability of the FBG sensor are considered, it is more convenient to measure strain with the FBG sensor in the individual layers of the CFRP laminate.

Although there are numerous studies on the usage of FBG sensors for different purposes in the literature,[10,20,22,29,30] to the best of the authors' knowledge, there is no study on measuring the slight strain variations caused by thermal expansion through FBG sensors by embedding them inside the different layers of a carbon fiber reinforced polymeric laminate and verification of this measured small strain with CLT. This theory is used to predict the residual stresses in carbon fiber-reinforced bismaleimide polymeric composites.[31] In another study, CLT successfully predicts the quasi-static elastic modulus of fused deposition modeling 3-D printed Polyethylene terephthalate glycol (PETG) polymer.[32] Moreover, CLT is used to predict the developed stress with respect to applied strain for fused deposition method-based 3-D printed polylactic acid (PLA) samples.[33]

FBG sensors are embedded in carbon fiber-reinforced aerospace-grade prepregs, which are stacked; and then cured in an autoclave. The manufactured laminate is then exposed to a temperature ramp with dwell times in a conditioning chamber to simulate temperature variation that actual composite structures might be exposed to throughout its service. Then, a small thermal strain is measured in the different layers of composite laminate with the FBG sensor by subtracting the effect of temperature on the central wavelength of the FBG sensors. The CLT verifies experimental strain measurement with embedded FBG sensors. While measuring the strain with the embedded FBG sensors, the top surface strain of the laminate is also being measured with a resistive strain gauge at

the same time in order to compare it with the values calculated by CLT.

1.1 | Fiber Bragg grating sensor

An FBG sensor serves as a pass-band filter where a broadband wavelength spectrum is sent to the FBG sensor through an interrogator, and only a narrow spectrum of the incoming wavelengths is reflected while most of the spectrum passes to the FBG sensor region. The reflected narrow spectrum is composed of the Bragg wavelengths distribution, and the wavelength with maximum reflectivity is called the center Bragg wavelength (λ_B). The condition for the Bragg wavelength is given as

$$\lambda_B = 2n_{eff}\Lambda \tag{1}$$

where Λ is the grating period, and n_{eff} is the effective refractive index of the FBG sensor. When an FBG sensor experiences a change in strain or temperature, the Bragg wavelength (λ_B) shifts. The following Equation can be used to relate the change in strain or temperature with the shift in Bragg wavelengths (λ_B)

$$\frac{\Delta\lambda_B}{\lambda_B} = (\alpha+\xi)\Delta T + (1-p_e)\epsilon \tag{2}$$

where $\Delta\lambda_B$ is the shift in the Bragg wavelengths, ΔT is the change in temperature, ϵ is the strain developed on the FBG sensor, p_e is an effective photo-elastic constant for silica fiber, α is the thermal expansion coefficient, and ξ is the thermo-optic coefficient of the optical fiber. The value of effective photo-elastic constant (p_e) for silica fiber is taken as 0.22.[28] The summation of the thermal expansion coefficient and thermo-optic coefficient ($\alpha+\xi$) is $6.67\times10^{-6}{}^{\circ}\mathrm{C}^{-1}$.[28]

The center wavelength of an FBG sensor is affected by the change in strain field and temperature. If the temperature is constant and a mechanical load is applied, still, mechanical strain is responsible for the shift in the center wavelength. But in this case, Equation (2) reduces to $\Delta\lambda_B/\lambda_B = (1-p_e)\epsilon$ and strain can be calculated easily. However, when the shift in the center wavelength of an FBG sensor is due to both temperature difference and mechanical strain, the temperature effect needs to be compensated for accurate strain measurement with an FBG sensor because the term thermal expansion coefficient (α), and the thermo-optic coefficient (ξ) of the optical fiber also contributes the shift in the Bragg wavelength.

2 | THE MATHEMATICAL FORMULATION OF CLASSICAL LAMINATION THEORY FOR COMPOSITE LAMINATES

To calculate the strain variation inside a specific lamina of the composite laminate, the reduced stiffness coefficients (Q_{ij}) of a unidirectional lamina needs to be calculated. For that reason, materials constants called the elastic modulus in the direction of the fiber (E_{11}), perpendicular to the fiber (E_{22}), the major Poisson's ratio (ν_{12}), and the in-plane shear modulus (G_{12}) needs to be known.

Transformed reduced stiffness coefficients ($\overline{Q}_{ij}$) of each lamina is related to reduced stiffness coefficients (Q_{ij}) of a unidirectional lamina and the angle of the lamina (θ). Once reduced stiffness coefficients (Q_{ij}) are calculated, then six independent transformed, reduced stiffness coefficients ($\overline{Q}_{ij}$) of each lamina can be determined by the sets of Equation (3).[34]

$$\begin{aligned}
\overline{Q}_{11} &= Q_{11}c^4 + Q_{22}s^4 + 2(Q_{12}+2Q_{66})s^2c^2,\\
\overline{Q}_{12} &= (Q_{11}+Q_{22}-4Q_{66})s^2c^2 + Q_{12}\left(s^4+c^4\right),\\
\overline{Q}_{22} &= Q_{11}s^4 + Q_{22}c^4 + 2(Q_{12}+2Q_{66})s^2c^2,\\
\overline{Q}_{16} &= (Q_{11}-Q_{12}-2Q_{66})c^3s - (Q_{22}-Q_{12}-2Q_{66})s^3c,\\
\overline{Q}_{26} &= (Q_{11}-Q_{12}-2Q_{66})cs^3 - (Q_{22}-Q_{12}-2Q_{66})s^3c,\\
\overline{Q}_{66} &= (Q_{11}+Q_{22}-2Q_{22})s^2c^2 + Q_{66}\left(s^4+c^4\right),
\end{aligned} \tag{3}$$

where $\mathrm{s} = \sin\theta$, and $\mathrm{c} = \cos\theta$. After that, to set a relation between the fictitious thermal loads and induced thermal strain in the midplane of the lamina, the extensional stiffness matrix ([A]), the coupling stiffness matrix ([B]), and the bending stiffness matrix ([D]) for a laminate can be calculated by Equations (4), (5), and (6), respectively.

$$A_{ij} = \sum_{k=1}^{n}\left[\left(\overline{Q}_{ij}\right)\right]_k\left(h_k - h_{k-1}\right), \mathrm{i}=1,2,6; \mathrm{j}=1,2,6 \tag{4}$$

$$B_{ij} = \frac{1}{2}\sum_{k=1}^{n}\left[\left(\overline{Q}_{ij}\right)\right]_k\left(h_k^2 - h_{k-1}^2\right), \mathrm{i}=1,2,6; \mathrm{j}=1,2,6 \tag{5}$$

$$D_{ij} = \frac{1}{3}\sum_{k=1}^{n}\left[\left(\overline{Q}_{ij}\right)\right]_k\left(h_k^3 - h_{k-1}^3\right), \mathrm{i}=1,2,6; \mathrm{j}=1,2,6 \tag{6}$$

The fictitious thermal loads (N) and moment resultants (M) because of induced thermal strain can be calculated by using Equations (7) and (8), respectively. External mechanical effects do not cause these fictitious

loads and moment resultants; however, they developed because of the induced thermal strain which is caused by the temperature.

$$[N] = \begin{bmatrix} N_x \\ N_y \\ N_{xy} \end{bmatrix} = \Delta T \sum_{k=1}^{n} \begin{bmatrix} \overline{Q}_{11} & \overline{Q}_{12} & \overline{Q}_{16} \\ \overline{Q}_{12} & \overline{Q}_{22} & \overline{Q}_{26} \\ \overline{Q}_{16} & \overline{Q}_{26} & \overline{Q}_{66} \end{bmatrix} \begin{bmatrix} \alpha_x \\ \alpha_y \\ \alpha_{xy} \end{bmatrix}_k (h_k - h_{k-1}) \quad (7)$$

$$[M] = \begin{bmatrix} M_x \\ M_y \\ M_{xy} \end{bmatrix} = \frac{1}{2}\Delta T \sum_{k=1}^{n} \begin{bmatrix} \overline{Q}_{11} & \overline{Q}_{12} & \overline{Q}_{16} \\ \overline{Q}_{12} & \overline{Q}_{22} & \overline{Q}_{26} \\ \overline{Q}_{16} & \overline{Q}_{26} & \overline{Q}_{66} \end{bmatrix} \begin{bmatrix} \alpha_x \\ \alpha_y \\ \alpha_{xy} \end{bmatrix}_k (h_k^2 - h_{k-1}^2) \quad (8)$$

Where ΔT is the temperature difference, α_x, α_y, and α_{xy} are the coefficient of the thermal expansion for lamina, h_k is the bottom surface location of a corresponding lamina and h_{k-1} is the top surface location of a corresponding lamina. Once fictitious loads and moment resultants are calculated, a relation between the fictitious loads, moments, midplane strains (ε_x^0, ε_y^0,γ_{xy}^0) and curvatures (κ_x, κ_y, κ_{xy}) can be established (Equation 10). Through established relation (Equation 10), fictitious loads and moment resultants, [A], [B], [D] matrices are known. Therefore, six independent equations from Equation (9) with unknown midplane strains and curvatures can be generated.[34,35]

$$\begin{bmatrix} N_x \\ N_y \\ N_{xy} \\ M_x \\ M_y \\ M_{xy} \end{bmatrix} = \begin{bmatrix} A_{11} & A_{12} & A_{16} & B_{11} & B_{12} & B_{16} \\ A_{12} & A_{22} & A_{26} & B_{12} & B_{22} & B_{26} \\ A_{16} & A_{26} & A_{66} & B_{16} & B_{26} & B_{66} \\ B_{11} & B_{12} & B_{16} & D_{11} & D_{12} & D_{16} \\ B_{12} & B_{22} & B_{26} & D_{12} & D_{22} & D_{26} \\ B_{16} & B_{26} & B_{66} & D_{16} & D_{26} & D_{66} \end{bmatrix} \begin{bmatrix} \varepsilon_x^0 \\ \varepsilon_y^0 \\ \gamma_{xy}^0 \\ \kappa_x \\ \kappa_y \\ \kappa_{xy} \end{bmatrix} \quad (9)$$

The induced thermal strain at any point of a laminate through the thickness can be calculated by Equation (10).[36]

$$\begin{bmatrix} \varepsilon_x \\ \varepsilon_y \\ \gamma_{xy} \end{bmatrix} = \begin{bmatrix} \varepsilon_x^0 \\ \varepsilon_y^0 \\ \gamma_{xy}^0 \end{bmatrix} + z \begin{bmatrix} \kappa_x \\ \kappa_y \\ \kappa_{xy} \end{bmatrix} \quad (10)$$

Where z is the location of the lamina from the midplane, in order to calculate the final thermal strain on a lamina inside the laminate, the free lamina strain induced by the applied temperature needs to be calculated. Here, Equation (11) gives the single lamina strain (strain on the single lamina, which is not part of any laminate) induced by the temperature difference.[37]

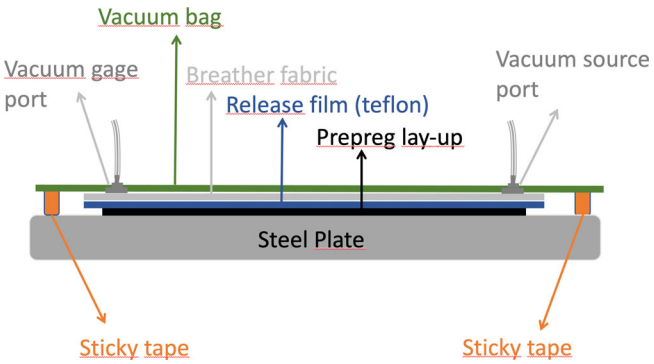

FIGURE 1 Bagging setup for autoclave curing.

$$\begin{bmatrix} \varepsilon_x^T \\ \varepsilon_y^T \\ \gamma_{xy}^T \end{bmatrix}_k = \begin{bmatrix} \alpha_x \\ \alpha_y \\ \alpha_{xy} \end{bmatrix}_k \Delta T \quad (11)$$

Then free lamina strain is subtracted from the induced thermal strain from a lamina inside the laminate to calculate the thermal strain which is given in Equation (12).

$$\begin{bmatrix} \varepsilon_x^M \\ \varepsilon_y^M \\ \gamma_{xy}^M \end{bmatrix}_k = \begin{bmatrix} \varepsilon_x \\ \varepsilon_y \\ \gamma_{xy} \end{bmatrix}_k - \begin{bmatrix} \varepsilon_x^T \\ \varepsilon_y^T \\ \gamma_{xy}^T \end{bmatrix}_k \quad (12)$$

Composite structures show a linear elastic behavior under small strains. The approach followed here is termed the Classical Lamination Theory, which assumes a linear elastic relation between stress and strain. Since this study aims to measure small variations in strain, the Classical Lamination Theory can be employed.

3 | METHODOLOGY

3.1 | Materials and sample preparation

Unidirectional carbon fiber prepreg with an aerial weight of 300 gr/m^2 and a trading code of AX-6201XL-C is obtained from Kordsa Global. This prepreg is suitable for aerospace applications and, at the same time, the autoclave curing method, which is the composite laminate production method preferred by the aerospace industry.

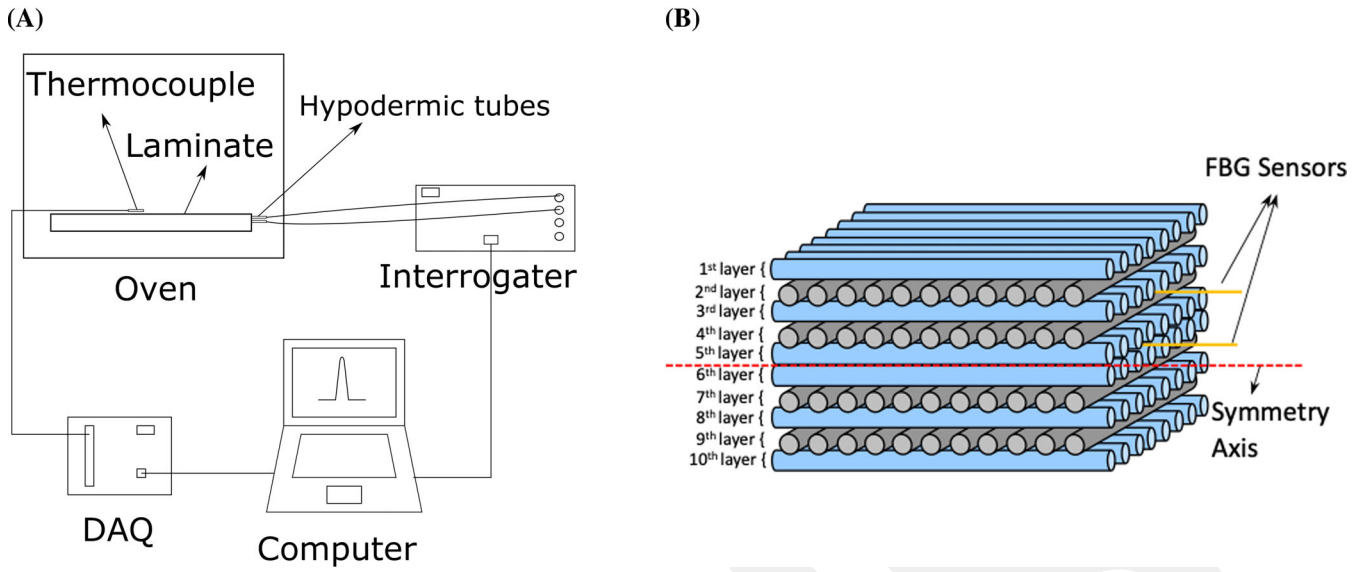

FIGURE 2 (A) Experimental setup, (B) locations of FBG sensors and stacking sequence of the laminate.

TABLE 1 Material elastic constant for the unidirectional carbon fiber lamina.

Elastic constants	Value	Standard
E_{11}	128 GPa	ASTM D 3039
E_{22}	7.7 GPa	ASTM D 3039
υ_{12}	0.289	ASTM D 3039
G_{12}	10.4 GPa	ASTM D 3518

For curing the laminate with an autoclave, first, the prepreg layers are cut in the dimension of $300 \times 300\ mm^2$ with a computer controller Digital Ply Cutter (ZÜND G3-L3200). Prepreg layers are layed-up in the form of a cross-ply stacking sequence on a steel plate, as shown in Figure 2B. Before laying up prepregs on the steel plate, four layers of release film are applied to the steel plate to prevent sticking between the plate and cured laminate. While laying up prepreg layers, two FBG sensors are placed between the prepreg layers, as shown in Figure 2B. The egress region of the FBG sensor from the stack of prepregs is provided with a hypodermic steel tube. The prepreg stack is covered with a non-perforated Teflon release film (Airtech WL5200). On top of the film, a layer of breather fabric (Airtech N10) is placed to provide air evacuation from the bagging setup. Then the whole setup is encircled with sticky tape (Airtech AT 200Y). A vacuum gauge port is placed on one end of the assembly, a vacuum source port is placed on the other end, and the whole assembly is sealed with a vacuum bag (Figure 1). Once every necessary step for a secure autoclave cycle is completed, a recipe is created based on the prepreg manufacturer's instructions, and the cycle is initiated.[38]

Once the cycle is completed, the autoclave lid is open, and when the air temperature inside the autoclave is reached 50°C. The autoclave cart is removed from the autoclave, and bagging consumables are cleared off from the cured composite laminate carefully to avoid damaging fiber optic cables.

3.2 | Mechanical characterization

While producing a carbon fiber-reinforced composite laminate with embedded FBG sensors, two more laminates are produced simultaneously to measure material elastic constants of the unidirectional lamina, which constitutes the laminate. These two plates have a stacking sequence of $[0]_4$ and $[45/-45]_{8s}$ and are tested as per ASTM D-3039 and ASTM D 3518 testing standards. Through ASTM D-3039 standard material elastic constants, elastic modulus in the direction of fiber (E_{11}), elastic modulus in the perpendicular direction to the fiber (E_{22}), the major Poisson's ratio ν_{12}, and with ASTM D 3518 in-plane shear modulus (G_{12}) are measured and tabulated in Table 1.

3.3 | Measurement of coefficient of thermal expansion

For the CLT, the coefficient of thermal expansion of the carbon fiber lamina needs to be determined in both parallel (α_1) and perpendicular (α_2) to the fiber direction.

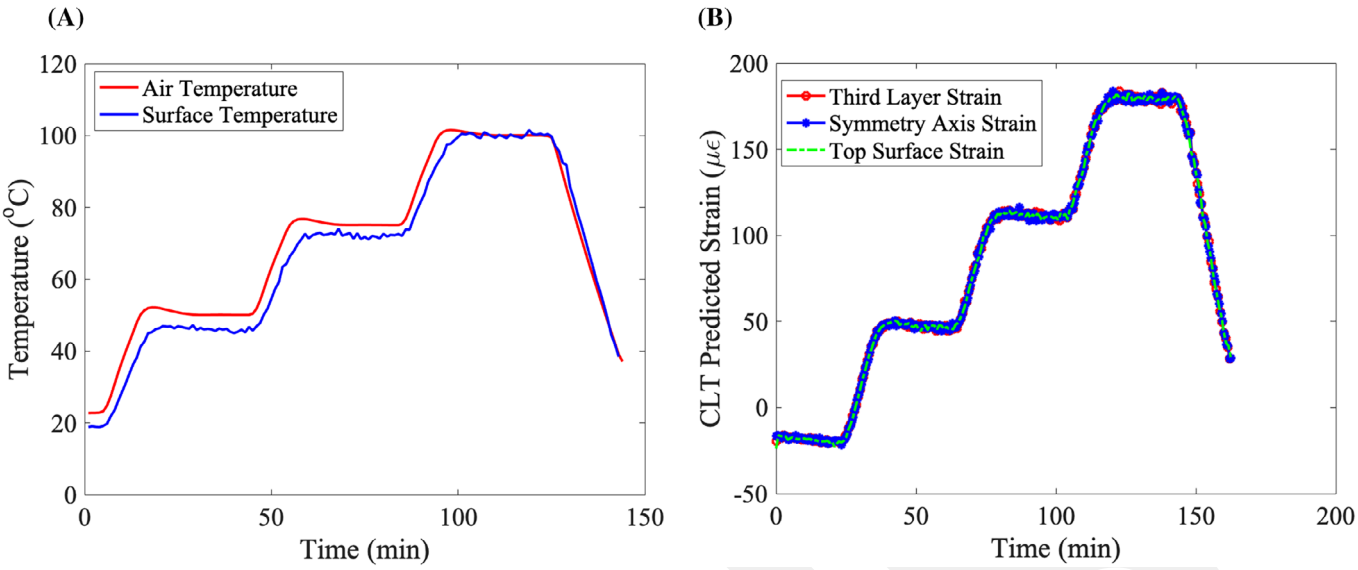

FIGURE 3 (A) Temperature evaluation inside the conditioning chamber and on the surface of the composite laminate, (B) CLT predicted strains in different layers.

Thermomechanical Analysis (TMA) (Mettler Toledo, TMA/SDTA 1+) is used to measure the coefficient of thermal expansion where the test is performed on the $50 \times 50 \times 1\,\text{mm}^3$ specimen of the unidirectional lamina. Samples are heated with a temperature ramp of $5°\text{C}/\text{min}$ and the coefficient of thermal expansions for two directions is calculated by fitting a curve passing through the 25°C and 100°C on the temperature-displacement curve obtained from TMA analysis. The coefficient of thermal expansions, α_1 and α_2, are calculated to be $0.61 \times 10^{-6}\text{m}/°\text{C}$ and $47.27 \times 10^{-6}\text{m}/°\text{C}$, respectively.

3.4 | Heating of composite plate within a conditioning chamber

The carbon fiber composite laminate is heated in a temperature and humidity conditioning chamber (Vötsch Technik clime-event). Prior to the experiment, absolute humidity is set to zero to reveal only the effect of temperature on the laminate. During the heating cycle, a K-type thermocouple and strain gauge is attached to the surface of the laminate to measure the temperature and strain on the top surface of the laminate. The thermocouple is connected to a National Instruments NI-PXIe-6363 DAQ card, and the strain gauge is connected to the NI-PXIe-4330 strain gauge card in a NI-PXIe-1075 chassis, and the thermocouple and strain gauge data are recorded through NI-Signal Express software. FBG sensors are illuminated with a Micron Optics SM 130 interrogator, and the reflected wavelengths are recorded with the same interrogator by using Micron Optics ENLIGHT software. The Micron Optics ENLIGHT software follows the central Bragg wavelength in the whole spectrum. Therefore, in this study, all calculation associated with FBG data is based on the central wavelength of the FBG sensor. The sampling rate of both interrogator and DAQ is set to 100 sample/s. The experimental setup can be seen in Figure 2A. The temperature ramp rate is set to $3°\text{C}/\text{min}$ and when the temperature is reached 50°C, 75°C, and 100°C, a dwell time of 30 min is given to reach a thermal equilibrium between the composite plate and the environment. The temperature evolution both for the air inside the conditioning chamber and the surface of the composite laminate can be seen in Figure 3A.

4 | RESULTS AND DISCUSSION

FBG sensors are embedded in different layers of an aerospace-grade carbon fiber reinforced laminate to assess the capability of FBG sensors for measuring thermally induced strain field therein. Thus, the laminate with embedded FBG sensors is exposed to temperature variations in a temperature-controlled conditioning chamber. The variation in the temperature inside the conditioning chamber and the surface of the composite laminate can be seen in Figure 3A. The temperature on the surface of the composite laminate gradually approaches the ambient temperature within the conditioning chamber, indicating that thermal equilibrium is attained towards the end of the heating cycle. The increase in the temperature of the laminate induces the same levels of thermal strains in each layer of the

laminate. This can be attained through the symmetric structure of the examined laminate. This numerical outcome can be supported by the experimental results, as seen in Figure 4, which depicts the mechanical strain reading of two embedded FBG sensors exposed to thermal stress within the examined laminate in two different layers. Even though there is around 60 με mechanical strain difference between the CLT and the experiment at 100°C, both FBG sensors and CLT reveals the same trend. This trend elucidates the correctness of FBG sensor reading for small strains when the FBG sensor is only exposed to thermal loading.

However, it is quite difficult to measure such small strains between the layers of a composite laminate. Only FBG sensors are capable of measuring the small strain values efficiently due to two significant advantages. First, the FBG sensor has a relatively small diameter (150 μm) which enables the embeddability of the FBG sensor in composite laminate to measure the strain in different layers without altering the mechanical properties of the laminate. Second, the FBG sensor is so sensitive that it can detect a strain change of approximately 1 με. Due to these reasons, FBG sensors are embedded in two different layers during the production step of the composite laminate.

An autoclave is a completely isolated pressured tube during the manufacturing process, and laminate can be exposed to a pressure of 7 bars and a temperature of 120°C, which is an extremely harsh environment. For such a production method, the embedment of FBG into the composite laminate is formidable because of the fragility of optic cables where FBG sensors are inscribed. However, despite all difficulties of the autoclave process, the laminate with embedded FBG sensors is produced successfully. Before curing the laminate in the autoclave and after the curing, the spectrum of FBG sensors is collected and exhibited in Figure 5A,B, respectively. Although a slight decrease is observed, the peak intensities of FBG sensors before and after the autoclave curing process are considered identical, which elucidates that with autoclave curing, FBG sensors can be successfully embedded into the composite laminate.

An insignificant residual strain remains on the composite laminate after autoclave curing, and it can vary from layer to layer. Residual strain in different layers of the laminate induced during the manufacturing procedure is measured by comparing the center wavelengths

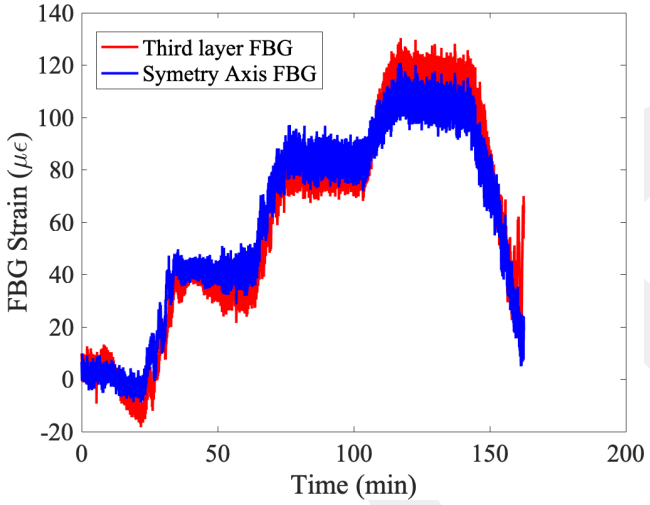

FIGURE 4 Strain reads by third layer and symmetry axis FBG sensors.

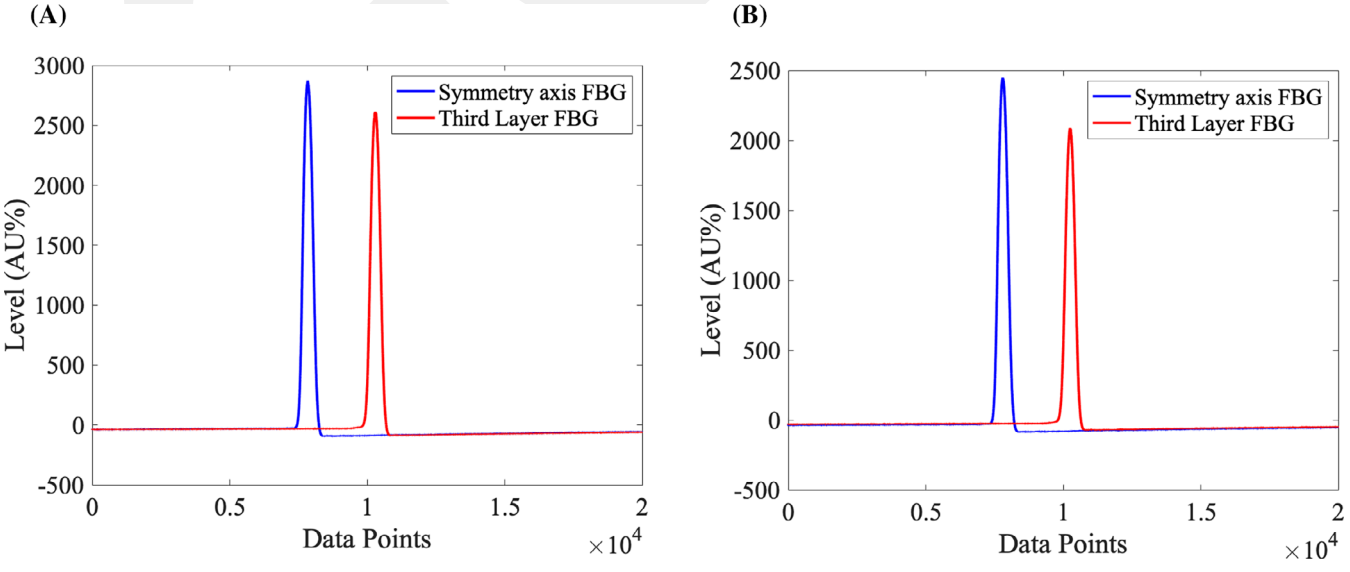

FIGURE 5 Spectrum of FBG sensors, (A) before the autoclave curing process, (B) after the autoclave curing process.

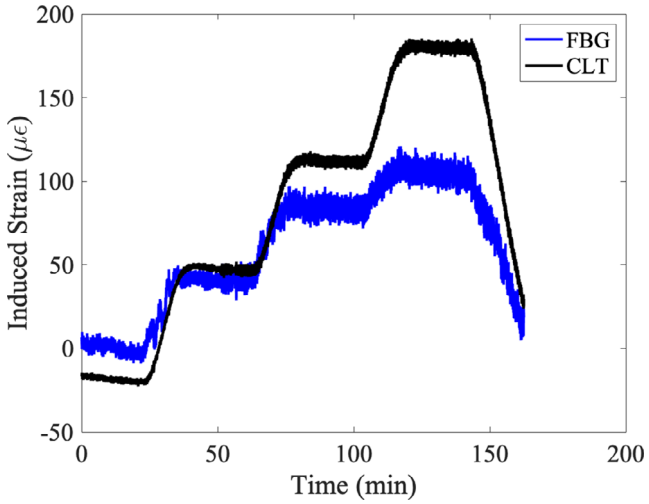

FIGURE 6 Strain measured by FBG and calculated by CLT for the bottom surface of the third layer.

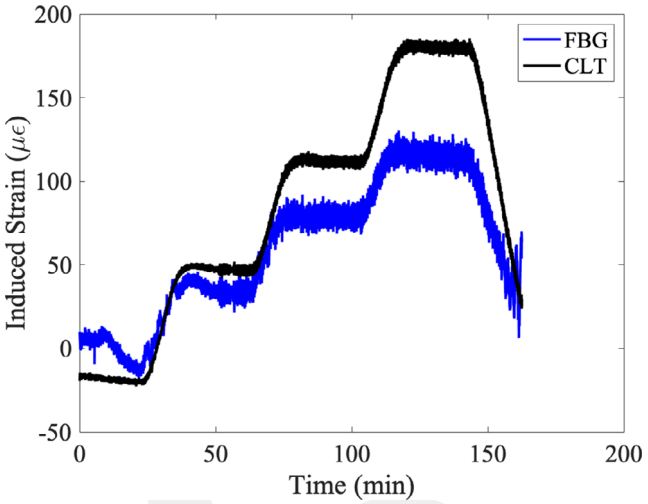

FIGURE 7 Strain measured by the FBG and calculated by the CLT for the symmetry axis.

of the FBG sensor recorded before and after the curing process. A depreciation of 0.1531 nm and 0.2025 nm center wavelengths are measured for the FBG sensor on the symmetry axis and the third layer, respectively. This depreciation in the center wavelength of the FBG sensors corresponds to shrinkage of 127.5 and 167.4 με on the symmetry axis and the third layer, respectively.

The strain readings obtained from the FBG sensor and strain calculated by CLT for the third layer are depicted in Figure 6. When the cooling starts, the thermal strain reads by the FBG sensor and calculated by CLT indicate a decreasing trend immediately. Until 75°C temperature, the strain values measured by the FBG and CLT agree well. When the temperature reaches 100°C, the strain read by the FBG sensor indicates lower values than that of the CLT.

The thermal strain reading of the FBG sensor and thermal strain calculated by CLT for symmetry axis lamina is shown in Figure 7. Up to 100°C, the strain calculated by CLT slightly overestimates the strain measured by the FBG sensor, yet both follow the same trend. However, when the temperature reaches 100°C, the FBG sensor and the CLT possess similar strain values. When the cooling step is initiated, CLT and FBG strain readings indicate a decreasing strain trend due to the contraction of the composite laminate.

Although it is more evident in Figure 7, the strain values read by the FBG sensors in the first part of the graph (just before heating starts) show a slightly decreasing trend, as seen in Figures 6 and 7. This slight decrease stems from resetting the relative humidity inside the oven before the heating process starts. As the relative humidity decreases, laminate contracts, and this contraction is being read by FBG sensors as a decrease in the strain.

To validate that an FBG sensor measures strain more accurately even at a wide range of temperature levels, a strain gauge is attached to the surface of the top layer of the laminate, and the strain measured by the strain gauge is compared with the one calculated through the CLT. Figure 8 shows that the strain values recorded by the strain gauge are inconsistent with the strain values predicted by the CLT. When the temperature inside the conditioning chamber is 50°C, the strain measured by the strain gauge is 200 με; however, for the same temperature, the strain calculated by CLT is only about 50 με, which implies an error of 300%. At the point where the temperature of the conditioning chamber is 75°C, the thermal strain measured by the strain gauge is 375 με, and the thermal strain calculated by CLT for the exact temperature is around 125 με; this difference corresponds to an error of 200%. Similarly, at 100°C, the strain reading of the strain gauge becomes 500 με, whereas the CLT indicates only a strain of 200 με, and the difference is equal to the 150% error.

It can be clear that there is a considerable difference between the strain reading of a strain gauge and the CLT when the temperature differences become significant. Even for this measurement, temperature compensation for the strain gauge is made with Equation (13), which is mentioned in the datasheet of the strain gauge.

$$\varepsilon_{comp} = -7.41 \times 10^{1} * T^{0} + 5 \times 10^{0} * T - 8.57 \times 10^{-2} * T^{2} + 3.95 \times 10^{-4} * T^{3} - 4.46 \times 10^{-7} \times T^{4} \quad (13)$$

where ε_{comp} is the amount of self-thermal expansion of the resistive strain gauge (in με) due to the applied

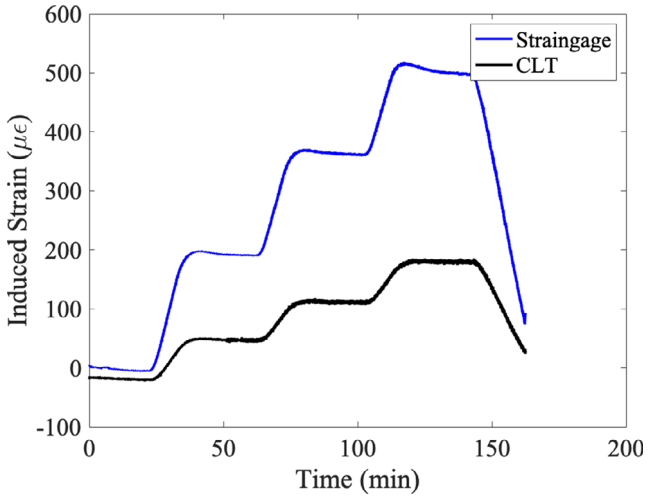

FIGURE 8 Strain measured by strain gauge and calculated by CLT for the top surface of the top layer.

temperature, while T is the temperature (in °C). The strain values measured by the strain gauge in Figure 8 are calculated by subtracting the self-thermal expansion of the resistive strain gauge from the total strain measured by the strain gauge.

When the strain read by the FBG sensor and strain gauge is compared, it can be easily seen that the reading of the FBG sensor closely matches Classical Lamination Theory. Therefore, it is deduced that the reading of the FBG sensor is more reliable than the strain gauge. In the literature, such a comparison of strain reading for FBG sensor and strain gauge for such an experimental setup (only considering the temperature as a cause for strain) is not available. However, the comparison between the strain reading of the FBG sensor and strain gauge can be found for the different experimental setups. In one of the early publications of Yilmaz et al.[18] a significant difference between the transverse strain (in the order of 500 με), as well as axial strain reading (in the order of 5000 με) of the FBG sensor and strain gauge, is reported during the quasi-static cyclic tensile test. The difference in the strain readings of the FBG sensor and strain gauge is also given by Akay et al.[19] during the fatigue testing of glass fiber-reinforced polymeric composites. Kocaman et al.[23] also reported a significant variation in the reading of the surface-adhered strain gauge and embedded FBG sensor. This variation in the strain reading of the FBG sensor and strain gauge is attributed to the formation of local strain variations as well as the position of the two sensors, such that the strain gauge is surface mounted; however, the FBG sensor is embedded. Apart from fiber-reinforced composites, debonding of the solder connections between the flip chip ball grid and printed circuit board by measuring strain by strain gage and surface mounted FBG sensor in the four-point bending test is analyzed. And it is seen that there are considerable differences between the strain gauge and FBG sensor.[39] In all of these experiments,[18,19,23,39] the temperature is kept constant, and there is an external load. When there is not any temperature change in the test piece, the cause of the strain is only external load, and sensors only measure the mechanical strain that develops on the test piece. However, herein, two contributions to strain are measured by both sensors. One contributor is the expansion of the test piece; the other one is the self-expansion of the sensor. The latter causes errors if a temperature compensation procedure is not used. Herein, the temperature compensation is used for both sensors yet there is a significant deviation for the strain gauge from the classical lamination theory as well from the reading of the FBG sensor.

5 | CONCLUSION

This study aims to analyze the sensitivity of embedded FBG sensors to measure the small strain variations under the influence of temperature. For that purpose, FBG sensors are successfully embedded into two different layers in an aerospace-grade carbon fiber prepreg stack, and the prepreg stack is cured inside an autoclave by being exposed to a temperature ramp. The strain developed in the different layers of the laminate due to temperature is monitored by the FBG sensors. A CLT is derived to verify the strain measurement of FBG sensors in the different layers under the temperature effect, which considers fictitious thermal loads and moment results to calculate thermal strain. The thermal expansion coefficient of the unidirectional lamina is experimentally measured with TMA and later used in the CLT. The thermal strain is calculated with CLT by considering the exact temperature cycle applied in the experiment. Finally, the strain measured by FBG sensors and the strain calculated by the CLT is compared. Based on the experimental results and observations, the following conclusions are drawn from this study. First, FBG sensors are successfully embedded and used to monitor the residual strain after curing composite laminate inside an autoclave. Second, CLT is effectively employed for the thermal strain calculation of a composite laminate in different layers. Third, even though strain variations are very small (με), embedded FBG strain readings are accurate for different layers and correlate with the strain calculated by the CLT. Fourth, the strain reading of the surface-attached resistive strain gauge does not agree with CLT as well as the reading of FBG sensors.

ACKNOWLEDGMENTS

The authors would like to acknowledge the partial support from Sabanci University Integrated Manufacturing Technologies Research and Application Center.

DATA AVAILABILITY STATEMENT

The data that support the findings of this study are available from the corresponding author upon reasonable request.

ORCID

Çağatay Yılmaz https://orcid.org/0000-0002-8063-151X

REFERENCES

[1] J. Lowe, *Woodhead Publ. Ser. Text*, Woodhead Publishing, Cambridge, UK, **2005**, p. 405. https://doi.org/10.1533/9781845690823.405

[2] M. Mrazova, *Incas. Bull.* **2013**, *5*, 139.

[3] R. R. Boyer, J. D. Cotton, M. Mohaghegh, R. E. Schafrik, *MRS Bull.* **2015**, *40*, 1055.

[4] J. Chen, J. Wang, X. Li, L. Sun, S. Li, A. Ding, *Compos. Struct.* **2020**, *242*, 112168.

[5] H. Hu, D. Cao, M. Pavier, Y. Zhong, L. Zu, L. Liu, S. Li, *Compos. Struct.* **2018**, *202*, 1361.

[6] J. Molimard, S. Vacher, A. Vautrin, *Strain* **2011**, *47*, 364.

[7] B. Seers, R. Tomlinson, P. Fairclough, *Polym. Compos.* **2021**, *42*, 1631.

[8] C. Zhang, G. Zhang, J. Xu, X. P. Shi, X. Wang, *Polym. Compos.* **2022**, *43*, 3350.

[9] J. R. Dunphy, G. Meltz, F. P. Lamm, W. W. Morey, *Proc.SPIE* **1990**, *1370*, 116. https://doi.org/10.1117/12.24834

[10] V. M. Murukeshan, P. Y. Chan, L. S. Ong, L. K. Seah, *Sensors Actuators A Phys.* **2000**, *79*, 153.

[11] K. Jung, K. T. Jin, *J. Compos. Mater.* **2007**, *41*, 1499.

[12] M. Yildiz, N. G. Ozdemir, G. Bektas, C. J. Keulen, T. Boz, E. F. Sengun, et al., *J. Manuf. Sci. Eng.* **2012**, *134*, 044502.

[13] F. Colpo, L. Humbert, J. Botsis, *Compos. Sci. Technol.* **2007**, *67*, 1830.

[14] N. Yadav, K. Wachtarczyk, P. Gąsior, R. Schledjewski, J. Kaleta, *Polym. Compos.* **2022**, *43*, 1590.

[15] S. S. Kim, H. Murayama, K. Kageyama, K. Uzawa, M. Kanai, *Compos. Part A: Appl. Sci. Manuf.* **2012**, *43*, 1197.

[16] H.-S. Kim, S.-H. Yoo, S.-H. Chang, *Compos. Part B Eng.* **2013**, *44*, 446.

[17] C. J. Keulen, E. Akay, F. F. Melemez, E. S. Kocaman, A. Deniz, C. Yilmaz, T. Boz, M. Yildiz, H. S. Turkmen, A. Suleman, *J. Intell. Mater. Syst. Struct.* **2014**, *27*, 17.

[18] C. Yilmaz, C. Akalin, E. S. Kocaman, A. Suleman, M. Yildiz, *Polym. Test.* **2016**, *53*, 98.

[19] E. Akay, C. Yilmaz, E. S. Kocaman, H. S. Turkmen, M. Yildiz, *Mater* **2016**, *9*, 9.

[20] A. Papantoniou, G. Rigas, N. D. Alexopoulos, *Compos. Struct.* **2011**, *93*, 2163.

[21] S. Mohanta, Y. Padarthi, J. Gupta, S. Neogi, *Polym. Compos.* **2021**, *42*, 4717.

[22] E. S. Kocaman, E. Akay, C. Yilmaz, H. S. Turkmen, I. B. Misirlioglu, A. Suleman, M. Yildiz, *Mater* **2017**, *10*, 10.

[23] E. S. Kocaman, C. Yilmaz, A. Deniz, M. Yildiz, *J. Sandw. Struct. Mater.* **2016**, *20*, 553.

[24] J. Seyyed Monfared Zanjani, B. Saner Okan, C. Yilmaz, Y. Menceloglu, M. Yildiz, *Compos. Part A: Appl. Sci. Manuf.* **2017**, *99*, 221.

[25] M. O. H. Cioffi, A. S. C. Bomfim, V. Ambrogi, S. G. Advani, *Polym. Compos.* **2022**, *43*, 7643.

[26] A. Kefal, I. E. Tabrizi, M. Yildiz, A. Tessler, *Mech. Syst. Signal Process.* **2021**, *152*, 107486.

[27] A. Kefal, I. E. Tabrizi, M. Tansan, E. Kisa, M. Yildiz, *Compos. Struct.* **2021**, *258*, 113431.

[28] A. D. Kersey, M. A. Davis, H. J. Patrick, M. LeBlanc, K. P. Koo, C. G. Askins, M. A. Putnam, E. J. Friebele, *Fiber Grating Sensors. J. Light Technol.* **1997**, *15*, 1442.

[29] C. Y. Wei, S. W. James, C. C. Ye, R. P. Tatam, P. E. Irving, *Strain* **2000**, *36*, 143.

[30] J. D. Pearson, M. A. Zikry, M. Prabhugoud, K. Peters, *Polym. Compos.* **2007**, *28*, 381.

[31] L. Di Landro, A. Palonca, G. Sala, *Polym. Compos.* **1995**, *16*, 276.

[32] X. Cui, J. P.-Y. Ben, *SPE Polym.* **2023**; n/a. https://doi.org/10.1002/pls2.10085

[33] C. YİLMAZ, H. Q. ALİ, M. YILDIZ, *Afyon Kocatepe Üniversitesi Fen Ve Mühendislik Bilim Derg* n.d., **2022**, *22*, 342.

[34] A. K. Kaw, *Mechanics of composite materials*, CRC Press, Boca Raton, Florida, **2005**.

[35] P. Qiao, J. F. Davalos, *Uddin NBT-D in F-RP (FRP) C for CE*, Woodhead Publ. Ser. Civ. Struct. Eng., Woodhead Publishing, Cambridge, UK, **2013**, p. 469. https://doi.org/10.1533/9780857098955.2.469

[36] R. Haynes, J. Cline, B. Shonkwiler, E. Armanios, *Compos. Sci. Technol.* **2016**, *127*, 20.

[37] X. Zhao, S. Sun, Y. Wang, X. Wang, *Mater. Res. Express* **2021**, *8*, 125307.

[38] H. Q. Ali, Ç. Yilmaz, M. Yildiz, *Polym. Test.* **2022**, *111*, 107612.

[39] H. Lu, R. Hussain, M. Zhou, X. Gu, *IEEE Sensors J.* **2009**, *9*, 457.

How to cite this article: Ç. Yılmaz, H. Q. Ali, M. Yıldız, *Polym. Compos.* **2023**, *44*(5), 2956. https://doi.org/10.1002/pc.27293